Phys. Status Solidi A **213,** No. 7, 1751–1759 (2016) / **DOI** 10.1002/pssa.201532806

physica status solidi a
www.pss-a.com
applications and materials science

Reliability aspects of hydrogen-doped indium oxide

Gabrielle C. E. Jost*, Alexander N. Hamri, Florian Köhler***, and Jürgen Hüpkes******

IEK-5 Photovoltaik, Forschungszentrum Jülich GmbH, 52425 Jülich, Germany

Received 1 October 2015, revised 1 March 2016, accepted 1 March 2016
Published online 22 March 2016

Keywords damp heat degradation, doping, hydrogen, In_2O_3, transparent conductive oxides

* Corresponding author: e-mail jost.gabrielle@googlemail.com, Phone: +49 2461 61 6310, Fax: +49 2461 61 3735
** e-mail alexander.hamri@rwth-aachen.de Phone: +49 152 53 29 18 17, Fax: +49 2461 61 3735
*** e-mail f.koehler@fz-juelich.de, Phone: +49 2461 61 5392, Fax: +49 2461 61 3735
**** e-mail j.huepkes@fz-juelich.de, Phone: +49 2461 61 2594, Fax: +49 2461 61 3735

We demonstrate an alternative route to reliably prepare hydrogen-doped indium oxide (In_2O_3:H). The common hydrogen source, water vapor, was substituted in our process by hydrogen and oxygen gas. The resulting films showed similar optical and electrical properties. Nevertheless, the process using gaseous hydrogen led to a simplification of the deposition process. By replacing the hydrogen source we increased the reproducibility of the electrical film properties significantly, thus, paving the way for a reliable device implementation of the material. Furthermore, we investigated the degradation behavior of In_2O_3:H under damp heat conditions as preliminary test for long-term durability in photovoltaic devices. The results revealed a degradation of the electrical properties that differs in detail regarding the amorphous and polycrystalline material. In the amorphous material, the main degradation is caused by loss of charge carriers, whereas in the polycrystalline material a drop of the charge carrier mobility causes a significant rise of the resistivity. However, we show that the relative degradation of the In_2O_3:H films is similar to other transparent contacts that are implemented in solar cells. Finally, we demonstrate that the degradation of the charge carrier mobility in the polycrystalline In_2O_3:H films is completely reversible by vacuum annealing at 200 °C.

1 Introduction Hydrogen-doped indium oxide (In_2O_3:H) has attracted a lot of attention as new contact material for silicon-based solar cells. Successful applications in silicon hetero-junction solar cells as well as silicon thin-film solar cells have already been reported [1–5]. The common fabrication procedure involves sputter deposition at room temperature using an indium oxide target with oxygen gas and water vapor as dopant source. The hydrogen-doped indium oxide layer is amorphous in the as-deposited state and changes into a polycrystalline phase upon an annealing step at relatively low temperatures (around 200 °C) [6]. It is this polycrystalline phase after annealing that shows outstanding electrical performance with high charge carrier mobility and low charge carrier density. Hence, In_2O_3:H is a promising candidate for transparent conductive oxides (TCO) applications that require high conductivity and at the same time good infrared transparency. Additionally, the low preparation temperatures make it an interesting choice for low temperature applications such as deposition onto temperature-sensitive devices or in electronics on plastic substrates, etc.

Various studies have been carried out using water vapor as dopant source and annealing temperatures around 200 °C in vacuum to initialize crystallization. However, the results reported by several groups vary. Fluctuations in the charge carrier density range from 1.1×10^{20} to 2.1×10^{20} cm^{-3} and charge carrier mobility between 98 and 140 $cm^2 V^{-1} s^{-1}$ within publications [5–9]. Additionally, stability problems of the water vapor flow during the process have already been reported by another group [10]. Hence, the water vapor process proved not reproducible enough to incorporate it reliably into any deposition sequence for an optoelectronic device.

In this work, we demonstrate the substitution of water vapor by hydrogen and oxygen gas in the process to enable a reproducible incorporation of high quality In_2O_3:H films into photovoltaic devices. The successful usage of hydrogen

gas as dopant source during sputter deposition was already shown by other groups for ITO [11] or zinc oxide [12, 13]. In addition to reproducibility, stability is an important factor for successful device integration. The targeted application in solar cells always involves a certain exposure to harsher ambient conditions than laboratory storage. Damp heat degradation tests are a standard method to investigate the degradation behavior of an entire solar module. However, the degradation behavior of the In_2O_3:H has been rarely investigated in literature before [14]. Therefore in the second part of this work, the stability of the deposited In_2O_3:H in damp heat environment as pre-stage of degradation within a photovoltaic device was investigated as well as possible recovery approaches.

2 Experimental All In_2O_3:H thin films were deposited in sputter deposition system constructed by Kurt J. Lesker Company Ltd. The sputter coater was equipped with a 6″ In_2O_3 target with 99.99% purity. The process gasses used were argon, a 10% hydrogen mixture in argon, and a 10% oxygen mixture in argon. The water vapor was supplied by a glass flask that was filled with deionized water. The glass flask was attached to the deposition system with an additional pumping station. The water vapor flow was controlled via a needle valve. To ensure the maximum reproducibility, the needle valve always was adjusted to the same partial pressure of water vapor at the beginning of the process using a standardized procedure including fixed stabilization periods. The hydrogen fraction that is used as independent variable in the course of this work was calculated using the flow ratios of the gases involved in the deposition. The water fraction on the other hand was calculated using the partial pressure ratios.

According to the dopant source, the samples are further on either referred to as H_2O or H_2 samples. The deposition pressure was kept constant at 0.27 Pa for all series. The chosen plasma excitation mode was radio frequency (RF) at 13.56 MHz, the generator power output was either 80 or 120 W. The annealing was performed in vacuum ($<10^{-6}$ mbar) within the sputter deposition system at a temperature of 200 °C for 20 min. Corning Eagle XG glass was used as substrate material for all tests shown. The thickness of the analyzed In_2O_3:H thin films was in the range of 120 nm. The exact thin-film thickness was assessed with a Dektak 6M Stylus Profiler by Veeco. The step for thickness measurements was prepared either with a simple etching step in 10% hydrochloric acid or with the rip off of vacuum proof Kapton® tape that was attached to the substrate surface prior to deposition. Charge carrier mobility and concentration as well as the resistivity were extracted from Hall measurements in van der Pauw geometry at room temperature using an RH2010 setup of PhysTech GmbH. The magnetic field strength was 820 mT during the measurement. Optical characterization was performed with a Perkin Elmer Lamda 950 UV/VIS Spectrometer. Transmission and reflection were both measured. The absorption was calculated using the measured transmission and reflection data under the assumption of energy conservation.

Structural information was derived from X-ray diffraction measurements in parafocussing Bragg Brentano geometry with a D8 Advance X-ray diffraction setup by Bruker Corporation using the K_α radiation of a Cu anode as the X-ray source. Data were recorded at scattering angles 2θ between 20° and 65° in ambient air. The step width amounted to 0.01° and the integration time was 2 s per step. The damp heat degradation was investigated applying standard test conditions based on IEC 61215: 85% relative humidity at a temperature of 85 °C. The damp test was performed for up to 1939 h in a commercially available climate chamber type NCC 4020 by NEMA Industrietechnik GmbH.

3 Results and discussion

3.1 Hydrogen/oxygen mixture as substitute for water vapor To enable a better stability and reproducibility of the deposition process, we first investigated the use of hydrogen gas instead of water vapor as dopant source. Using hydrogen gas is advantageous as normal mass flow controllers can be applied to adjust the gas flow accurately during the process. The results of Hall effect measurements (charge carrier mobility, charge carrier density, and resistivity) of a comparative study of both deposition methods are shown in Fig. 1. All samples were deposited with the same deposition conditions with regard to the deposition pressure 0.27 Pa and generator power 120 W and annealed for 20 min at 200 °C. Only the gas mixture was changed among the processes. The samples in Fig. 1a–c were deposited with a mixture of argon (Ar), oxygen (O_2), and hydrogen gas (H_2). The O_2-flow was adapted to the H_2-flow to yield a ratio of H_2:O_2 of 2:1, thus imitating stoichiometric water. The samples in Fig. 1d–f on the other hand were deposited with the classical method using argon, water vapor (H_2O), and an additional O_2 ratio of 0.3%. Note that the total oxygen atomic ratio in the plasma is composed of water and oxygen gas. Thus, in case of water vapor sputtering the conditions are slightly more oxidic than for the sputtering process with the hydrogen/oxygen gas mixture. Here the results are presented as a function of the H_2 ratio or H_2O ratio, accordingly. The as-deposited samples are illustrated with blue squares whereas the corresponding-annealed samples are shown as red triangles. Both test series show a dependence of the Hall parameters on the H_2 respective H_2O ratio. In the as-deposited state, the mobility increases with the addition of H_2 or H_2O, respectively, when compared to the intrinsic sample. An increase is also visible for the charge carrier density, however, it decreases again when a H_2, respectively, water vapor ratio of about 1% is surpassed. In case of the water vapor depositions, the absolute charge carrier densities of the intrinsic sample at 0% dopant ratio are lower than those of the 0% H_2 intrinsic reference sample. This is most likely due to the additional 0.3% O_2 ratio in the H_2O deposition process leading to charge carrier compensation. Low charge

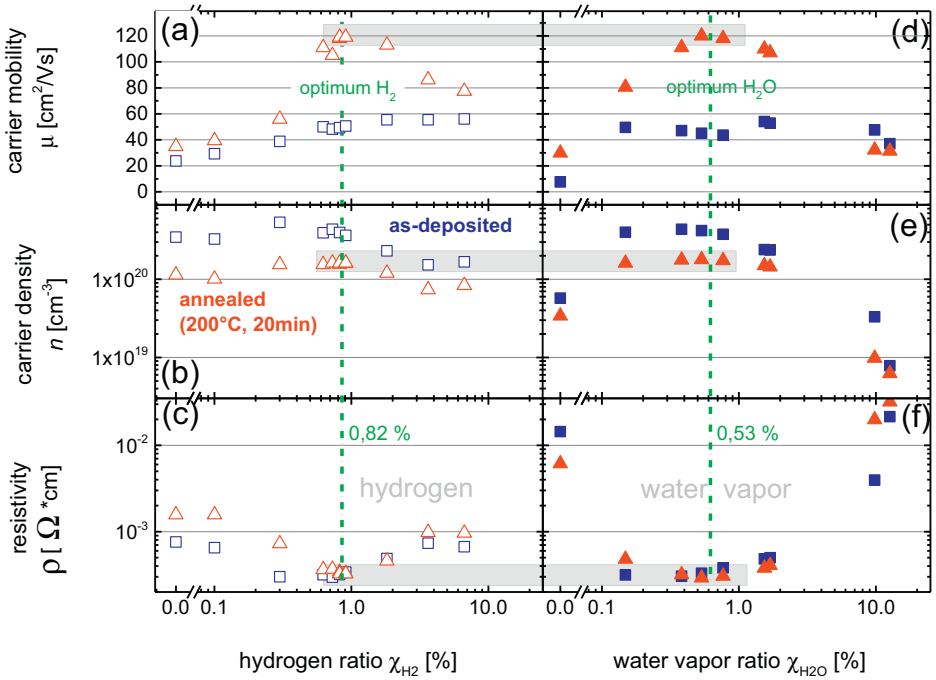

Figure 1 Electrical properties of In_2O_3:H films; (a) charge carrier mobility, (b) charge carrier density, (c) resistivity as a function of hydrogen ratio (χ_{H2}) during deposition. Electrical properties of In_2O_3:H films; (d) charge carrier mobility, (e) charge carrier density, and (f) resistivity as a function of water vapor ratio (χ_{H2O}). Blue squares represent the as-deposited films, red triangles correspond to vacuum-annealed films. All films prepared with H_2 were deposited with an H_2:O_2-ratio of 2:1 to correspond with stoichiometric H_2O. All films deposited with H_2O vapor contained an additional O_2-ratio of 0.3%. The optimum doping source ratio and corresponding resulting electrical properties are represented by a green dash-dotted line and the shaded area, respectively.

carrier densities below the intrinsic value were also achieved with very high H_2O ratio (10%). In this case, two effects could be involved. The high amount of water vapor in the plasma will draw power from the plasma, hence there is less power remaining for the actual sputtering process. We have also seen in additional tests (not shown) that the deposition rate dropped by more than 30%. The amount of O_2 in the plasma remained unchanged and thus there is more oxygen relative to In_2O_3. Additionally, H_2O is still split in the plasma, releasing even more oxygen. Hence, an increased oxygen content in the film and therefore a compensation of free electrons is likely.

Similar effects could not be reproduced with the H_2 doping. As the O_2 amount was always adapted to the H_2 ratio (2:1), the gas mixture limited the maximum H_2 ratio to 6.7%. After the annealing step, the charge carrier mobility increased whereas the charge carrier density dropped. This behavior is widely known from literature for the films deposited with H_2O [5–7]. Both deposition methods showed an optimum range marked in Fig. 1 with a green dash-dotted line where the resistivity in the as-deposited as well as the annealed state reached its minimum. Although the optimum films were deposited at different oxygen fraction, the doping ratio range between about 0.6 and 1% each charge carrier mobility surpassed $120\,cm^2\,V^{-1}\,s^{-1}$ and the charge carrier density dropped to about $2 \times 10^{20}\,cm^3$ for both deposition methods. Hence, the electrical performance was the same for both methods and in the range of values reported in literature for H_2O-based processes [5–9]. However, SIMS analysis (not sown) revealed that the H content of the optimal films deposited with H_2 is about 23% lower than the one in H_2O-based films. One reason for the different incorporation of H_2 could be that the H_2 molecule dissociates differently in plasma deposition processes. Additionally, it is not clear whether hydrogen is incorporated as atomic hydrogen or as an entire OH-group. The latter highly electronegative molecule is known to be a common dissociation product when splitting H_2O in plasma [15]. There are a number of theoretical studies on the configuration of hydrogen in indium oxide [16, 17]. They reveal interstitial or substitutional hydrogen on an oxygen site as shallow donor. Additionally, hydrogen incorporated at grain boundaries is considered as passivation of defects to reduce the transport barrier [7, 14, 18–20].

During the annealing, SIMS measurements revealed that a small fraction of the hydrogen (about 10%) effused (not shown). Even though this cannot explain the reduction of free electrons by a factor of two, a similar drop is commonly observed during the crystallization of In_2O_3:H [7, 19]. This effect might be related to the defect passivation by hydrogen at grain boundaries without an active doping effect.

To confirm the alikeness between the properties of the both types of In_2O_3:H films deposited, additional optical

measurements were performed. Figure 2 shows transmission and reflection measurements and the calculated absorption spectrum. The corresponding arithmetic mean values (400–1200 nm) are listed in Table 1. The measured layers were deposited in the optimum range of each deposition method with a dissipated power of 80 W. Blue lines show as-deposited films, red lines show the corresponding-annealed films. Dashed lines represent the films with H_2, solid lines the films with H_2O as dopant source. The absorption in the near infrared region dropped when both films were annealed. The drop is due to a reduced free carrier absorption that stems from the decrease in charge carrier density upon annealing. At the same time, the absorption edge experienced a blue shift due to the crystallization process. Although the difference in charge carrier density causes slight differences in the optical behavior of both films before the annealing process, the results after the annealing process are almost identical.

The different oxygen fraction in the plasma (we have added 0.3% of oxygen gas in case of the H_2O process) did not alter the electrical and optical properties for optimized films. In fact, the higher oxygen fraction in the water-based process lead to slightly higher charge carrier density and free carrier absorptance in the as-deposited state.

As the structure of the In_2O_3:H after the annealing step is the key to the excellent electrical performance, XRD measurements of films deposited in the optimum H_2O process and optimum H_2 process were performed. The results are shown in Fig. 3(a and b: H_2O; c: $H_2 + 1/2\ O_2$). The additional results in (d) will be discussed in Section 3.2. The cubic powder reference spectrum is displayed in (e). While the as-deposited sample in (a) does not show any crystalline phase, a polycrystalline phase is clearly visible for both annealed films. The peak positions correspond to

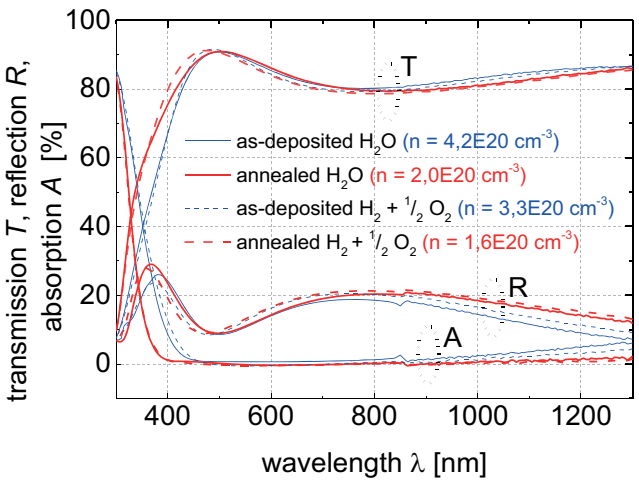

Figure 2 Transmission (T), reflection (R), and absorption (A) of In_2O_3:H films deposited with H_2O (solid lines) and H_2 (dashed lines) as a function of wavelength. All samples were deposited in the optimum gas flow ratios of the respective process with a dissipation power of 80 W and without an additional O_2-ratio.

Table 1 Average transmission (T), reflection (R), and absorption (A) of as-deposited and annealed In_2O_3:H films on glass from Fig. 2.

		as-deposited		annealed	
	unit	H_2O	H_2	H_2O	H_2
T	%	83.4	82.9	82.9	82.4
R	%	14.6	16.0	16.8	17.5
A	%	1.9	1.1	0.3	0.1

the cubic powder reference, however, the peaks show a variation in relative intensities indicating a preferential orientation, which is different for the two types of films. Remarkably, we did not find an obvious relation between preferential orientation and electrical properties. Nonetheless, both layer types have a polycrystalline structure which was also reported in literature as premise for a good electrical quality [6].

Both as-deposited films in the optimum range of doping ratio did not show any crystalline peak in XRD

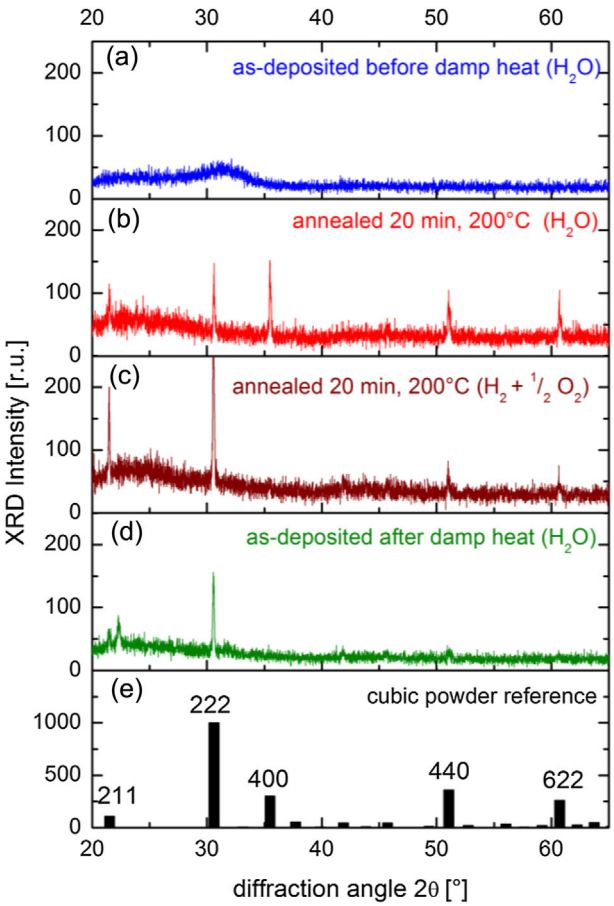

Figure 3 Diffraction pattern of as-deposited H_2O-based film (a), annealed H_2O-based film (b), annealed H_2-based film (c), as-deposited-film after 967 h damp heat treatment (d). All diffraction patterns were measured in Bragg–Brentano geometry. The diffraction peaks of an In_2O_3 cubic powder sample are displayed in (e) as additional reference.

diffractograms. The reason for the different texture in the annealed state remains unclear. However, this is consistent with literature data, that also report on different crystalline textures for high mobility In_2O_3:H films. Macco et al. [20] report on 400 textured films, while Koida et al. [7] demonstrate optimized In_2O_3:H with a rather random orientation.

Thus, we have reproduced the beneficial electrical as well as optical properties of hydrogen-doped indium oxide using both deposition routes with H_2O vapor and H_2/O_2 gas mixture, respectively.

The advantage of the alternative deposition method lies in the strongly enhanced reproducibility of the resulting film properties. Figure 4 shows the electrical parameters of a series of depositions (A, B, C, ...) that were all conducted with nominally identical deposition conditions. Parts (a), (b), and (c) depict the charge carrier mobility, charge carrier density, and resistivity of films deposited with the H_2-based method, whereas parts (d), (e), and (f) show the corresponding results of In_2O_3:H films deposited with the H_2O method. Each series of deposition runs extended over more than 1 month and more than 100 other depositions at different conditions or of different materials. The base pressure before each deposition was between 4.5 and 9.0×10^{-7} mbar.

The differences in the average values of charge carrier density and charge carrier mobility between the two processes are due to the slight differences in deposition conditions as the H_2-based process was further optimized

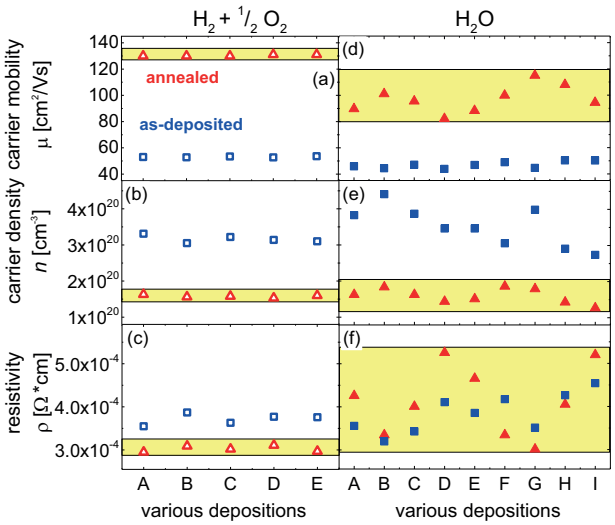

Figure 4 Electrical properties of hydrogen-doped indium oxide; (a)/(d) charge carrier mobility, (b)/(e) charge carrier density, and (c)/f) resistivity for various deposition runs. Blue squares represent as-deposited films, red triangles annealed films. The yellow bars indicate the scattering range of the electrical properties of the annealed films. All films prepared with H_2 were deposited with an H_2:O_2 ratio of 2:1 to correspond with stoichiometric H_2O at a discharge power of 80 W. All films deposited with H_2O vapor contained an additional O_2-ratio of 0.3% and were deposited at 120 W.

(see figure caption). However, the lack in reproducibility of the H_2O-based process is clearly visible in the spread of the electrical parameters. As visual aid, the yellow bars indicate the spread in electrical properties of the annealed films with both deposition methods. Exemplary, the resistivity values fluctuate between 3×10^{-4} and 5×10^{-4} Ωcm after the annealing step whereas the H_2-based process yields stable resistivity values around 3×10^{-4} Ωcm for all samples. Table 2 shows the standard deviations for the electrical parameters shown in Fig. 4 and illustrates the drastic improvement in reproducibility of electrical parameters when changing the dopant source in the process. In the annealed state, for example, the standard deviation of the resistivity is lowered by more than one order of magnitude.

One reason for the instability of the H_2O process is the simple water glass flask/needle valve set-up that is used to control the H_2O ratio in the process. This set-up is very susceptible to ambient conditions like changing room temperature, which governs the actual H_2O vapor pressure in the flask, and preconditioning of the deposition system. Hence, the real H_2O vapor partial pressure in the deposition system may vary and drift slightly during the deposition process, although all controllable parameters were set to the same values at the beginning of the process. The technical challenges when stabilizing a very small H_2O vapor flow by a needle valve – already had been addressed in another indium oxide-related publication [10]. In this study, the variations in H_2O vapor partial pressure were reported to be up to half an order of magnitude. These drawbacks are avoided in the H_2-based approach as standardly calibrated mass flow controllers can be used to control the H_2 ratio most accurately and reproducibly.

3.2 Damp heat degradation of In_2O_3:H films

Applying In_2O_3:H in solar cells for power generation always implies an exposure of the device to ambient conditions over decades. Accelerated life time tests are commonly used to evaluate and estimate the degradation behavior. Damp heat tests have already shown that the electrical properties of conventional TCOs are subject to degradation [14, 21].

Figure 5 depicts the charge carrier mobility (a), charge carrier density (b), and resistivity (c) as a function of the damp heat exposure time. Note that each data point represents the average value of three samples that were

Table 2 Comparison of standard deviations of electrical properties for conventional H_2O-based process and new H_2-based process.

	as-deposited		annealed	
	H_2O (%)	H_2 (%)	H_2O (%)	H_2 (%)
ρ	11.1	3.0	18.5	2.1
n	14.8	2.9	12.2	2.2
μ	5.0	0.7	9.9	0.4

treated equally. Blue squares indicate as-deposited samples whereas red and green triangles indicate the samples that had been annealed before damp heat treatment. Samples deposited with H_2 (open symbols) as well as samples deposited with H_2O (closed symbols) were degraded to further investigate the comparability of films of both deposition processes. The resistivity of all samples increases with increasing damp heat exposure time. However, the degradation differs in detail with regard to the as-deposited and the annealed films. The as-deposited films show a strong decrease in the charge carrier density over time whereas the charge carrier mobility even increases for the sample deposited with H_2O. This increase is not visible for the as-deposited H_2-based sample though. The annealed samples on the other hand show a strong degradation of the charge carrier mobility. The charge carrier density on the other hand hardly decreased. All films share that the degradation is still proceeding after 1000 h.

The maximum damp heat duration tested within our experiments was 1939 h. Note the extension of the test period beyond the 1000 h defined by the IEC61646 regulation. The results of an annealed H_2O-based In_2O_3:H film are shown separately in Fig. 5 using green triangular data points. For the annealed H_2O-based samples, the main contribution to the electrical degradation was the loss in charge carrier mobility whereas the charge carrier density dropped only slightly. After 1939 h, the mobility drops even below the initial value that the samples normally show in the amorphous, as-deposited state before the annealing step is applied. In the as-deposited state, an annealing step for 20 min at 200 °C in vacuum had led to a drastic improvement of the charge carrier mobility (data points highlighted with a red ring). In an attempt to restore the electrical properties of the degraded sample, it was again annealed at standard conditions. After the recovery annealing, indicated by a green arrow in Fig. 5, the mobility reached the initial value before degradation. The charge carrier density drops again slightly during the annealing step. However, in combination the resistivity of the material is almost back to its original value. Note that the films were already crystallized before the damp experiments.

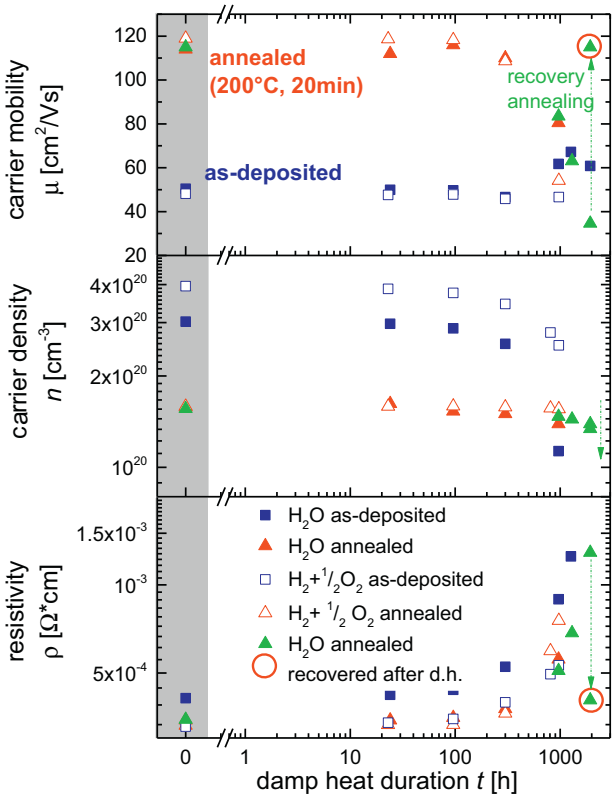

Figure 5 Damp heat degradation of the electrical properties; (a) charge carrier mobility, (b) charge carrier density, and (c) resistivity of hydrogen-doped indium oxide layers as a function of damp heat exposure time. Blue squares represent as-deposited films, red triangles annealed films. Closed symbols were deposited with H_2O, open symbols with H_2 as dopant source. Each data point represents the average value of three equally treated samples. Only the green data points show one single sample. The green data points that are highlighted with a red ring show the sample after the recovery annealing step.

In Fig. 6, a comparison of the relative changes in charge carrier mobility (a), charge carrier density (b), and resistivity of all investigated In_2O_3:H sample configurations after 967 h of damp heat exposure are shown. A reference H_2O-based series that was only exposed to 85 °C in nitrogen atmosphere is displayed in the yellow area of the graph. An additional reference layer is the Jülich-type ZnO:Al after 1000 h of degradation displayed with a hatched bar in the figure. Details of the Jülich-type ZnO:Al can be found in Ref. [22].

All tested films show an increase of the resistivity either related to a loss in charge carrier mobility or density after damp heat treatment. There is no clear indication whether the resistivity of either as-deposited or annealed In_2O_3:H samples degrades more under the influence of damp heat. In case of the H_2-based depositions, the as-deposited films degraded less than the annealed films whereas in case of the H_2O-based process the findings are contrary. The only improvement was the slight increase in charge carrier mobility of the as-deposited H_2O-based films.

Although, the charge carrier mobility increase is outweighed by the charge carrier loss at 967 h it is quite surprising to witness an improvement under these conditions at all. In Fig. 3, an XRD scan of the as-deposited film before the damp heat exposure (a) and after the exposure (d) shows a possible explanation. The originally amorphous layer (a) crystallized during the damp heat experiment (d). A polycrystalline structure is visible. The peak positions identified within (d) correspond to those of an In_2O_3 powder sample with cubic crystal structure (e). However, relative intensities reveal a polycrystalline nature with some suppressed orientations: for example (400), (440), and (622). When comparing these XRD results with the classical intentionally annealed H_2O-based sample (b) some differences in the intensity distribution of the peaks become quite obvious. Nevertheless, both films show a polycrystalline

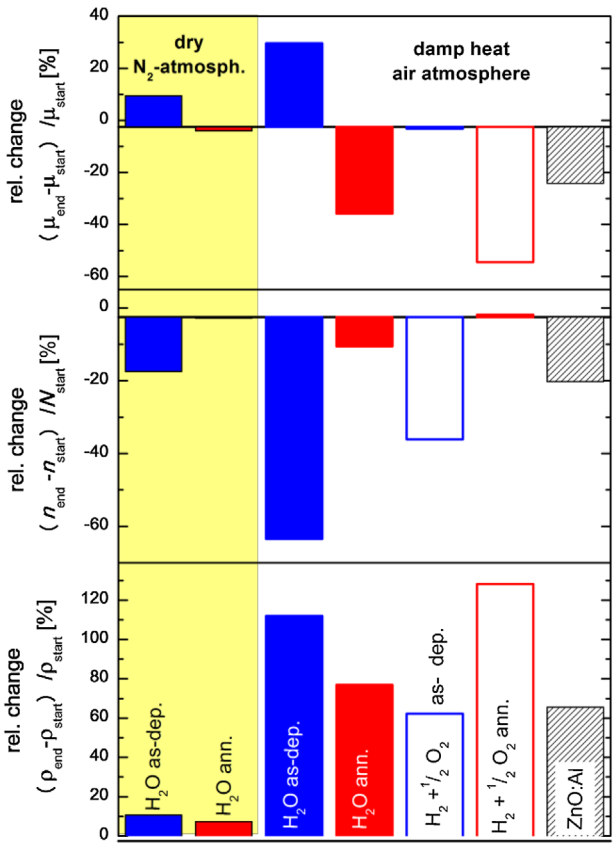

Figure 6 Relative change of (a) charge carrier mobility, (b) charge carrier density, and (c) resistivity of different thin-film materials after 967/1000 h of damp heat exposure time. A reference series (yellow area) that was exposed to 85 °C in nitrogen atmosphere only is also shown.

structure and therefore we can conclude the increase in charge carrier mobility during the damp experiment can be attributed to a slow way of crystallization that occurs in a similar way, when annealing the films comparatively rapidly after the deposition.

The samples that were exposed to 85 °C in nitrogen atmosphere showed the least degradation measured in the test. Thus we attribute the degradation effect in In_2O_3:H mainly to the ingress of H_2O, CO_2, or other atmospheric constituents into the grain boundaries and/or into bulk material in case of the amorphous films. The degradation in nitrogen might stem from residual atmospheric constituents that could not completely be eliminated in our experiment. In literature, it is claimed that the high mobility of crystalline In_2O_3:H is based on a reduced grain boundary scattering of charge carriers, where the grain boundaries are passivated by hydrogen [10]. Grain boundaries represent a natural percolation path for environmental atoms or molecules into the crystalline material. Chemical bonds, for example, hydroxides or carbonates that form at the grain boundaries could impair the previously mentioned passivation, thus, the scattering at the grain boundaries is drastically increased. Another study has shown similar effects dominant in the reduction of charge carrier mobility of aluminum-doped zinc oxide in damp heat atmosphere [23]. The charge carrier density of the crystalline In_2O_3:H film on the other hand stems from a doping effect of hydrogen within the grain and not the grain boundaries. As an external excess into the densely packed crystalline structure is rather unlikely, the charge carrier density is almost unchanged in the damp heat measurement.

The degradation behavior is different when looking at the amorphous material. The amorphous material is characterized by lattice distortions, bond angle fluctuations, and vacancies, thus naturally opening numerous percolation paths into and through the bulk material. Some of the atmospheric constituents can act as charge carrier trap, when entering the material, thus compensating the charge carrier concentration generated by the hydrogen doping. Another effect could be the chemical bond of the dopant hydrogen to the intruding species. These effects lead to the drastic decrease in charge carrier density visible for the amorphous films. Of course, each of these new traps also creates a fluctuation in the local potential, however, the effect on the charge carrier mobility is not as devastating as in the crystalline phase. A possible explanation could be that in case of the crystalline material, one can imagine each grain to be a highly conductive island surrounded by a grain boundary. If the potential barrier at the grain boundary rises tremendously, for example, due to the suggested chemical modification, the conductive island is surrounded by an "electric fence" that hinders the lateral charge carrier transport. In case of the amorphous material there are numerous paths for the electron through the material. Lattice distortions, vacancies and other kinds of traps create randomly distributed potential barriers. However, there are no predestined barrier lines insulating a certain area as in the crystalline material, on the contrary the random distribution always leaves alternative routes for the charge carrier transport. Thus, the degradation effect of the charge carrier mobility is minor in the amorphous phase.

The penetration and chemical reactions by environmental species could also explain the recovery annealing shown in Fig. 5. When heating the material after damp heat treatment, the thermal dehydration breaks these bonds and the atmospheric constituents effuse, thus restoring the original In_2O_3:H chemical configuration and hydrogen passivation at the grain boundaries. Similar recovery experiments after damp heat have also been reported for ZnO:Al. The charge carrier density and partially charge carrier mobility were restored after damp heat treatment using an annealing step in vacuum at 150 °C [24].

It can be stated that in our study, the increase in resistivity of the In_2O_3:H films upon damp heat exposure was higher than the one reported for related materials like ITO [25]. However, the degradation was in the same order of magnitude as the one of sputter deposited ZnO:Al films.

This is a remarkable result, because the reference ZnO:Al layer was deposited at substrate temperatures of 300 °C to yield compact material and was much thicker

ca. 800 nm (vs. ca. 115 nm In_2O_3:H). Thinner ZnO:Al layers tend to degrade more than thicker layers [26]. Additionally, the degradation of ZnO:Al deposited at temperatures below 200 °C can be expected to be stronger. In case of ZnO:Al, the deterioration of the electrical properties was attributed to penetration of and physi- or chemisorption with the humid atmosphere and residual gases [27]. Which particular element or molecule is responsible for the degradation is still under investigation. Though, CO_2 has been suggested as probable candidate to degrade ZnO:Al in the presence of water [26, 27], a recent investigation disproved the influence of small fractions of CO_2 [28]. As already pointed out, similar processes are likely to be involved in the degradation of In_2O_3:H as well. A similarity between the two materials is the necessity for humidity to initiate the severe degradation. However, in other studies an additional degradation mechanism for In_2O_3:H is supposed. The passivation of grain boundary defects by the H dopant is disrupted by adsorbed OH-radicals from the DH chamber, forming H_2O molecules that finally desorb [14].

Studies of ZnO:Al have shown, that a high temperature (650 °C) annealing could prevent the degradation. An explanation involved the grain boundaries that are supposed to be the main percolation path for an exchange with the ambient. According to Hüpkes et al. [24], the grain boundaries were sealed by the annealing step. However, this method could not be applied to In_2O_3:H because such high temperatures would lead to a hydrogen effusion up to a level where the In_2O_3:H films are electrically deteriorated already. Considering the findings and boundary conditions in the evaluation of our experiment, In_2O_3:H is a viable contact material for solar cell applications. We suppose this is valid for both deposition methods, because we do not expect a systematic difference. The slight variations might occur by slightly different film properties that might be optimized by adjustment of deposition parameters and annealing conditions.

4 Conclusions We introduced high quality hydrogen-doped indium oxide films deposited using a mixture of H_2 and O_2 gas. The electrical and optical results are similar to those of films prepared with the classical water vapor-based method. Furthermore, the new process shows an excellent reproducibility of film properties which is needed when targeting an industrial application. Damp heat experiments show that both as-deposited as well as annealed films experience electrical degradation. The degradation is bound to the presence of water. The effects that lead to an increase in the resistivity during damp heat differ in detail. In the as-deposited state, the charge carrier density drops significantly over time. The annealed films on the other hand show a strong decrease in charge carrier mobility but the charge carrier density decreases only slightly. The degradation of the resistivity in both cases is higher than the one reported for ITO but ranges in the same order of magnitude as the one already known for zinc oxide, a common TCO in photovoltaic application. We showed that the mobility degradation of the annealed films is almost completely reversible by a repetition of the vacuum annealing step at 200 °C. Concluding, we improved the reliability of the In_2O_3:H film properties by introducing a new deposition process and additionally, showed a viable long-term stability of this material thus paving the way for device integration.

Acknowledgements The authors would like to thank Alain Doumit and Wilfried Reetz for extensive technical support. This work was partially supported by the German Bundesministerium für Wirtschaft und Energie (BMWi) under contract number 0325299A (LIST project).

References

[1] T. Koida, H. Fujiwara, and M. Kondo, Appl. Phys. Express **1**, 041501 (2008).
[2] L. Barraud, Z. C. Holman, N. Badel, P. Reiss, A. Descoeudres, C. Battaglia, S. De Wolf, and C. Ballif, Sol. Energy Mater. Sol. Cells **115**, 151–156 (2013).
[3] T. Koida, H. Sai, and M. Kondo, Thin Solid Films **518**, 2930–2933 (2010).
[4] E. Moulin, M. Steltenpool, M. Boccard, L. Garcia, G. Bugnon, M. Stuckelberger, E. Feuser, B. Niesen, R. van Erven, J.-W. Schüttauf, F.-J. Haug, and C. Ballif, IEEE J. Photovolt. **4**, 1177 (2014).
[5] H. Scherg-Kurmes, S. Körner, S. Ring, M. Klaus, L. Korte, F. Ruske, R. Schlatmann, B. Rech, and B. Szyszka, Thin Solid Films **594**, 316–322 (2015).
[6] T. Koida, M. Kondo, K. Tsutsumi, A. Sakaguchi, M. Suzuki, and H. Fujiwara, J. Appl. Phys. **107**, 033514 (2010).
[7] T. Koida, H. Fujiwara, and M. Kondo, Jpn. J. Appl. Phys. Express Lett. **46**, L685 (2007).
[8] T. Koida, H. Fujiwara, and M. Kondo, Sol. Energy Mater. Sol. Cells **93**, 851 (2009).
[9] C. Battagglia, L. Erni, M. Boccard, L. Barraud, J. Escarré, K. Söderström, G. Bugnon, A. Billet, L. Ding, M. Despeisse, F.-J. Haug, S. De Wolf, and C. Ballif, J. Appl. Phys. **109**, 114501 (2011).
[10] H. F. Wardenga, M. V. Frischbier, M. Morales-Masis, and A. Klein, Materials **8**, 561 (2015), doi: 10.3390/ma8020561.
[11] S. Ishibashi, Y. Higuchi, Y. Ota, and K. Nakamura, J. Vac. Sci. Technol. A **8**, 1399 (1990), doi: 10.1116/1.576889.
[12] Y. Hu, Y. Chen, J. Chen, X. Chen, and D. Ma, Appl. Phys. A **114**, 875 (2014), doi: 10.1007/s00339-013-7733-0.
[13] M. L. Addonizio, A. Antonaia, G. Cantele, and C. Privato, Thin Solid Films **349**, 93 (1999).
[14] T. Tohsophon, A. Dabirian, S. De Wolf, M. Morales-Masis, and C. Ballif, APL Mater. **3**, 116105 (2015).
[15] S. V. T. Nguyen, J. E. Foster, and A. D. Gallimore, Rev. Sci. Instrum. **80**, 083503 (2009).
[16] P. D. C. King, R. L. Lichti, Y. G. Celebi, J. M. Gil, R. C. Vilão, H. V. Alberto, J. Piroto Duarte, D. J. Payne, R. G. Egdell, I. McKenzie, C. F. McConville, S. F. J. Cox, and T. D. Veal, Phys. Rev. B **80**, 081201 (2009).
[17] S. Limpijumnong, P. Reunchan, A. Janotti, and C. G. Van de Walle, Phys. Rev. B **80**, 193202 (2009).
[18] B. Macco, H. C. M. Knoops, and W. M. M. Kessels, ACS Appl. Mater. Interfaces **7**, 16723 (2015).
[19] H. Wardenga, M. Frischbier, M. Morales-Masis, and A. Klein, Materials **8**, 561 (2015).

[20] B. Macco, Y. Wu, D. Vanhemel, and W. M. M. Kessels, Phys. Status Solidi RRL **8**, 987 (2014).
[21] D. Greiner, N. Papathanasiou, A. Pflug, F. Ruske, and R. Klenk, Thin Solid Films **517**, 2291 (2009).
[22] M. Berginski, J. Hüpkes, M. Schulte, G. Schöpe, H. Stiebig, B. Rech, and M. Wuttig, J. Appl. Phys. **101**, 074903 (2007).
[23] K. Sago, H. Kuramochi, H. Iigusa, K. Utsumi, and H. Fujiwara, J. Appl. Phys. **115**, 133505 (2014).
[24] J. Hüpkes, J. I. Owen, M. Wimmer, F. Ruske, D. Greiner, R. Klenk, U. Zastrow, and J. Hotovy, Thin Solid Films **555**, 48 (2014).
[25] C. Guillen and J. Herrero, Surf. Coat. Technol. **201**, 309 (2006).
[26] T. Tohsophon, J. Hüpkes, S. Calnan, W. Reetz, B. Rech, W. Beyer, and N. Sirikulrat, Thin Solid Films **511–512**, 673 (2006).
[27] M. Theelen, S. Dasgupta, Z. Vroon, B. Kniknie, N. Barreau, J. van Berkum, and M. Zeman, Thin Solid Films **565**, 149 (2014).
[28] J. Hüpkes, Phys. Status Solidi A **213**, 1796–1800 (2016), this issue.